JOURNAL OF MATERIALS SCIENCE 32 (1997) 537–542

Microstructure and mechanical properties of a Si_3N_4/Al_2O_3 nanocomposite

W. Z. ZHU*, J. H. GAO, Z. S. DING
Department of Materials Science and Engineering, Institute of Inorganic Materials, Zhejiang University, Hangzhou, 310027, People's Republic of China

A nanocomposite material fabricated by hot pressing in the form of nanometre-sized Si_3N_4 particles dispersed in an Al_2O_3 matrix has been shown to exhibit enhanced mechanical properties compared with monolithic matrix material. It was observed by transmission electron microscopy (TEM) for the first time that the alumina grains were in the shape of elongated columns with aspect ratios in the range 2.5–4. The presence of liquid phase during sintering was found to be responsible for the appearance of columnar grains. Regular hexagon-shaped larger β′-Sialon grains formed during sintering were mainly situated at grain boundaries of the matrix material while irregular smaller dispersoids were trapped within the alumina grains. The improvement in the mechanical properties of the nanocomposite is attributed to the change in fracture mode from intergranular fracture to transgranular fracture, the ''self-reinforcement effect'' arising from the elongated columnar grains of the matrix, as well as the ''pinning effect'' due to the existence of intergranular β′-sialon particles. It was revealed that the trapped particles have an α-Al_2O_3 structure with partial sites of aluminium and oxygen atoms substituted by silicon and nitrogen atoms, which is also likely to lead to the strengthening of the composite.

1. Introduction

Ceramic-matrix nanocomposites have been increasingly receiving attention, primarily due to their significantly enhanced mechanical properties and low-temperature densification [1–5]. It was shown by Niihare and his colleagues in their pioneering work [6], that a bending strength as high as 1 GPa and a fracture toughness as high as 7 MPa $m^{1/2}$ can be obtained for the system where nanometre-sized SiC was dispersed in an Al_2O_3 matrix. The mechanism suggested by Niihare to be responsible for the improvement of the mechanical properties is an overall refinement of the microstructure resulting from the introduction of ultrafine SiC particles into alumina grains. The availability of nanometre-sized Si_3N_4 powder makes it possible to investigate the mechanical response of a nanocomposite of sub-micrometre Al_2O_3 reinforced with Si_3N_4, a system which is worth studying owing to the low thermal conductivity and low thermal expansion coefficient of Si_3N_4. In previous studies, much less attention has been paid to the microstructure of the interface between nanophase (reinforcement) and matrix in comparision with conventional ceramic matrix composites. The aim of the present work was to study the microstructure of Si_3N_4/Al_2O_3 nanocomposite, with emphasis intentionally put on the interface by means of high-resolution electron microscopy (HREM), in an attempt to correlate the mechanical behaviour with interfacial structure.

2. Experimental procedure

The α-Al_2O_3 powders doped with 0.25 wt % MgO with a mean particle size of 0.5 μm and amorphous Si_3N_4 powders with a mean particle size of 35 nm were employed in the present study. The alumina powders were synthesized from decomposition of chemically pure $(NH_4)_2Al_2(SO_4)_4 \cdot 2H_2O$ admixed with an aqueous solution of analytically pure $Mg(NO_3)_2$. The amorphous Si_3N_4 powders were prepared by plasma-induced chemical vapour deposition and contained > 37 wt %N, > 57 wt % Si and 2 wt % according to chemical analysis. 15 vol % Si_3N_4 particles were added to the Al_2O_3 starting powder, and the mixture was ultrasonically dispersed and then ball-milled in ethanol for 20 h. Both alumina and composite powders were calcined in air at 400 °C for 2 h in order to burn out any residual organics from powder processing. The calcined powders were placed into a graphite die which was lined with a boron nitride coating. The specimens were hot pressed at 1700 °C for 1 h under a pressure of 30 MPa in a flowing nitrogen atmosphere. For the sake of comparision, a monolithic alumina specimen was also prepared using the same processing technique as the composite.

Phase constituents of both matrix and composite materials were detected by using X-ray diffractometry (XRD) with a copper target and its K_α radiation. Density measurements were carried out using

* Author to whom all correspondence should be addressed.

0022–2461

Archimede's technique with an immersion medium of deionized water plus a wetting agent. The fracture toughness, K_{Ic}, was measured by the single-edge notched beam (SENB) method. The SENB specimen was in the form of a bending bar (2 mm × 4 mm × 22 mm) containing a chevron notch deeply cut in the centre and grooved on the flanks to ensure a stable mode of fracture. The notch was cut with a diamond blade 0.15 mm wide. Specimens were tested in three-point flexural geometry (16 mm) with a crosshead speed of 0.05 mm min^{-1}. Six specimens were used to obtain a statistical average value of fracture toughness. The flexural strength was measured by three-point bending. The size of the specimen was 3 mm × 4 mm × 36 mm with a polished surface as the tensile surface. The crosshead speed was 0.5 mm min^{-1} with a span of 30 mm. The strength values were calculated from the average of four tests. Specimens for TEM observation were prepared by grinding, dimpling, and ion-beam thinning followed by coating with a thin film of amorphous carbon. The JEM200X microscopy was employed with 200 KV as the accelerating voltage.

3. Results and discussion

3.1. Morphology of the matrix grains

XRD profiles of the composite and pure alumina are shown in Fig. 1a and b, respectively, from which it is evident that the composite contains two distinct crystalline phases, namely, α-Al_2O_3 and β-Si_3N_4. In view of the fact that starting powders of Si_3N_4 were amorphous, XRD results imply that the crystallization of Si_3N_4 powders has taken place during sintering. Compared with the XRD pattern of a pure alumina ceramics, the relative intensity of the peaks of the composite has obviously changed as shown in Table I. It is thus speculated that for composite material preferred grain growth along some planes of alumina occurred during sintering, which is not the case for pure alumina. It is rather intriguing to observe that almost all the alumina grains are in the form of elongated columns with aspect ratios in the range 2.5–4 as shown in Fig. 2. The unusual morphology of alumina grains in the Si_3N_4/Al_2O_3 nanocomposite, reported here for the first time, was only rarely mentioned in previous literature concerning alumina matrix nanocomposites. The grains of pure alumina appear to be elongated. It is the difference in the morphology of the alumina grains which makes the peak intensity of the composite different from that of pure alumina. In some cases, a thin glassy phase existing at the interface between alumina and intergranular grains was disclosed by HREM observation, as shown in Fig. 3. The starting materials of Al_2O_3, MgO, and particularly SiO_2 on the surface of contaminated Si_3N_4 powders, are likely to contribute to the formation of amorphous phase. The amount of this amorphous phase is believed to be rather small and broadening of peaks at small angles in XRD pattern,

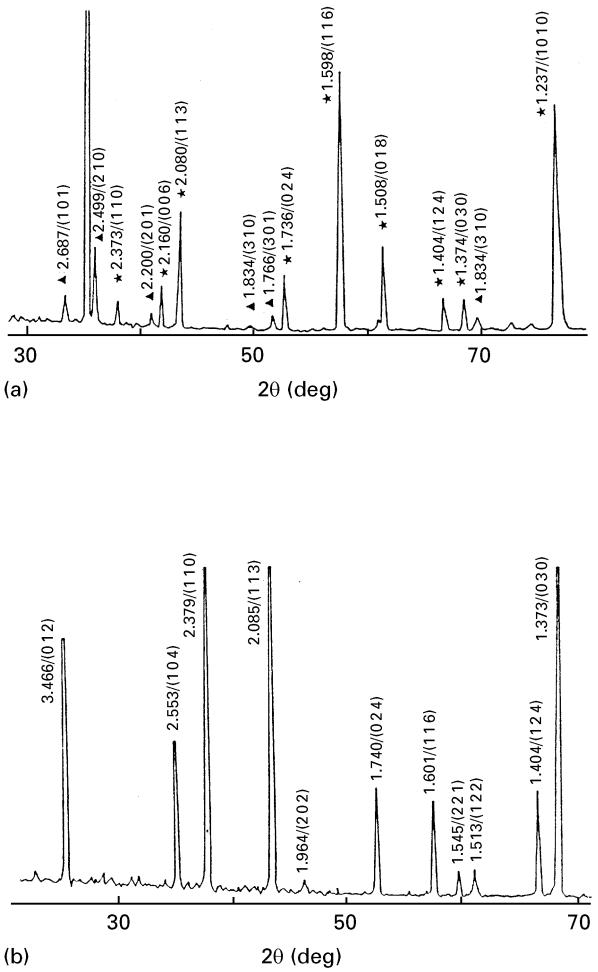

Figure 1 X-ray diffraction pattern of (a) the 15 vol % Si_3N_4/Al_2O_3 nanocomposite and (b) the pure alumina ceramics. (★) α-Al_2O_3, (▲) β-Si_3N_4.

TABLE I Relative intensity of the XRD peaks for alumina ceramic and Si_3N_4/Al_2O_3 nanocomposite

Materials	Strong peaks	Medium peaks	Weaks peaks
Al_2O_3 ceramic	(1 1 3), (1 1 0), (0 3 0), (0 1 2)	(1 0 4), (1 2 4), (0 2 4), (1 1 6)	(2 0 2), (2 2 1), (1 1 2)
Si_3N_4/Al_2O_3 nanocomposite	(1 0 4), (1 1 6)	(1 1 3), (2 1 0), (2 0 0), (0 2 1)	(1 1 0), (1 0 1), (2 0 1), (3 1 0)

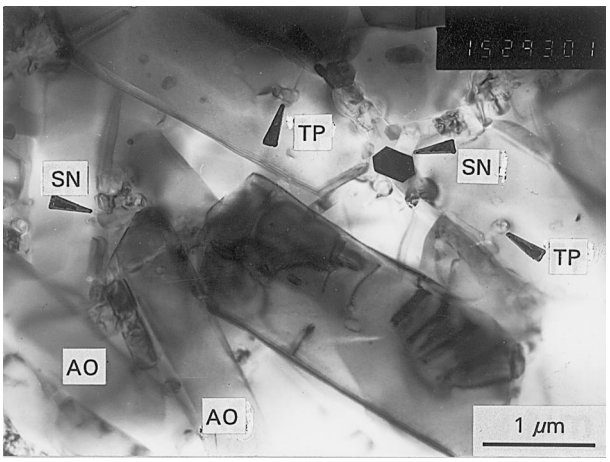

Figure 2 Transmission electron micrograph of the 15 vol % Si_3N_4/Al_2O_3 nanocomposite; AO, alumina; SN, Si_3N_4; TP, trapped particle.

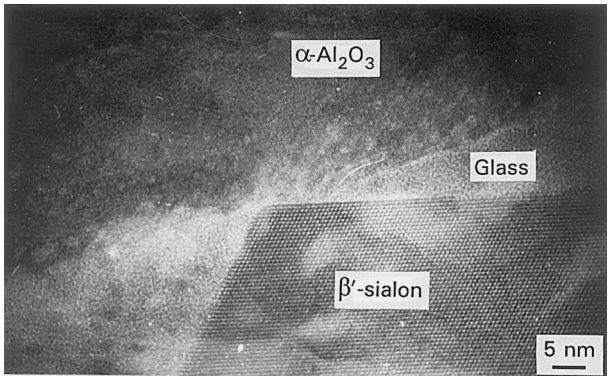

Figure 3 HREM lattice image on the interfaces between an alumina grain and an intergranular β′-sialon particle.

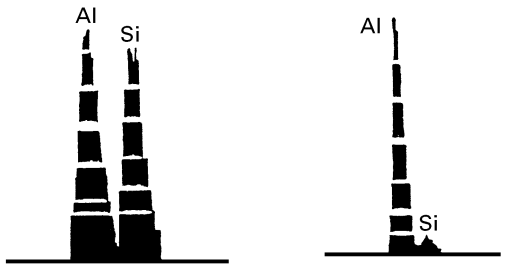

Figure 4 EDAX spectra of the 15 vol % Si_3N_4/Al_2O_3 nanocomposite: (a) nanoparticles in grain boundaries; (b) nanoparticles trapped in alumina grains.

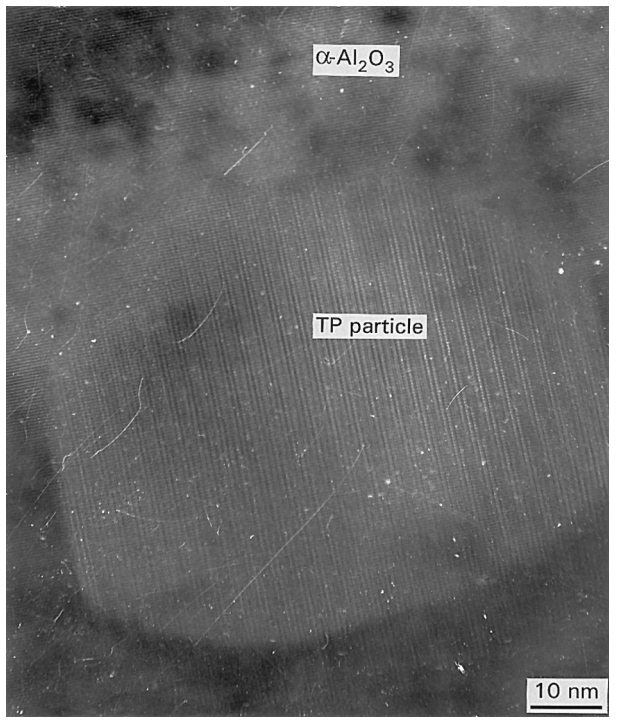

Figure 5 HREM lattice image of a trapped particle in an alumina grain.

which arises from the presence of glassy phase, cannot be detected. The phenomenon of the presence of liquid phase during high temperature sintering facilitating preferential growth of grains has been well investigated [7, 8]. Without exception in the present study, the liquid phase plays an important role in the formation of the elongated columnar grain microstructure during sintering.

3.2. Distribution of dispersed nanoparticles

It is apparent from Fig. 2 that two kinds of nanometre-sized dispersants exist in the composite, namely, inter- and intragranular particles. Regular hexagon-shaped larger particles of 200–300 nm in size are located primarily at matrix grain corners. These relatively coarser intergranular particles, which probably result either from hard aggregates contained in initial powders or grain growth during sintering, are seemingly β-Si_3N_4 crystallized from the starting amorphous powders. Electron probe microanalysis (EPMA) results of intergranular grains, which are shown in Fig. 4a, reveal that β-Si_3N_4 contains as much aluminium as silicon atoms. It is thus deduced that part of the silicon and nitrogen atoms have been replaced by aluminium and oxygen atoms during consolidation, resulting in the formation of β′-Sialon. Owing to the fact that β′-Sialon possesses the same hexagonal lattice system as β-Si_3N_4, it is not easy to distinguish them through XRD diffraction. Some irregular particles of about 80 nm in size were trapped within the alumina grains. Smaller β-Si_3N_4 particles were engulfed by several surrounding alumina grains, which eventually aggregated to become an individual grain during sintering. The morphology of intragranular nanometre-sized particles is therefore produced. Once the process of entrapment by matrix grains is complete, the growth of intragranular particles is severely retarded, which leads to smaller particle size compared with intergranular ones. Strain fringes, dislocation piles-up as well as micro-flaws around these trapped particles are occasionally observed [9], which are thought to be caused by residual stresses resulting from mismatch of thermal expansion coefficients between the matrix and reinforcement. The HREM photograph shown in Fig. 5 further reveals that the intragranular particles are different from intergranular ones in phase structure and appear to be an ordered substitutional solid solution of Si_3N_4 in an Al_2O_3 matrix. The trapped nanoparticles are supposed to be chemically active and easy to be completely dissolved in the liquid phase during sintering. Solid solution of Al_2O_3 containing an appreciable amount of Si_3N_4 is crystallized out during cooling, which can be further confirmed by the EMPA results shown in Fig. 4b, where the trapped particles are seen to contain a considerable content of silicon atoms.

3.3. Mechanical properties of the nanocomposite

Table II lists the mechanical properties of the nanocomposite. Both flexural strength and fracture toughness are significantly improved compared with those of monolithic alumina ceramics. Niihara and Nakahira [10] pointed out that the mechanical properties of several oxides and nitrides can be enhanced

TABLE II Mechanical properties of the 15 vol % Si_3N_4/Al_2O_3 nanocomposite

Materials	Density ($g\,m^{-3}$)	Flexural strength (MPa)	Fracture toughness ($MPa\,m^{1/2}$)
Alumina	3.95	380	3.91
Nanocompositè	3.90	820	6.00

by a dispersion of submicrometre SiC particles. An increase in strength from 380 MPa for alumina, up to 1 GPa for the system in which submicrometre SiC particles were located within the alumina, was reported, while the fracture toughness was also enhanced by about 40%. However, the mechanisms responsible for the enhancement of the mechanical properties are not well clarified. The present results further imply that besides SiC, Si_3N_4 can also be used as reinforcement to improve the mechanical properties of alumina, even if some chemical reaction has taken place. Scanning electron microscopy of the fracture surfaces has revealed a change in the fracture mode from intergranular for the monolithic alumina to a predominantly transgranular fracture for the composite material [11]. In the present study, despite the fact that grain boundary β′-Sialon phase has a lower thermal expansion coefficient than that of alumina, and is likely to open the matrix grain boundaries and intergranular fracture results, in practice, because a large amount of nanometre-sized particles are dispersed within the alumina grains, the intergranular fracture is negligible. Another possibility is that combined with glassy phase, β′-Sialon at the grain boundaries acts to strengthen the grain boundaries, which results in higher strength values. In this sense, intergranular particles possess a so-called "pinning effect". Because the thermal expansion coefficient of the trapped particles which are solid solutions of Si_3N_4 in α-Al_2O_3 is lower than that of the matrix material, internal stresses result on cooling with the nanoparticles compressed and with a general hydrostatic tensile stress in the matrix, on to which local stresses around the particles (tensile hoop stresses, radial compression) are superimposed. This is claimed to generate dislocation structures which become ordered to the extent of providing a set of linked subgrain boundaries between trapped particles. The result is an effective refinement of the microstructure from the submicrometre of the matrix to the nanoscale of the inclusion spacing. Consequently, transgranular fracture will be dominant.

3.4. Superlattice structure of intragranular particles

The HREM photograph of a trapped particle shown in Fig. 5 reveals that the alumina matrix and the trapped particle bond directly, with a high degree of coherency. It is believed that the interface between the matrix and the nanoparticle is actually semi-coherent with compensating dislocations wedged at the interface. Strong and weak lattice fringes periodically appear in the trapped particle. Table III lists some spacings between various crystal planes determined from the electron diffraction pattern (shown in Fig. 6) of the nanoparticle and the corresponding standard values of α-Al_2O_3 crystal. It is disclosed that the determined results are close to the standard spacings in regard to various crystal planes of α-Al_2O_3. In brief, the crystal structure of the trapped particle resembles that of α-Al_2O_3 which is hexagonal, but the EPMA profile in Fig. 4b demonstrates that the particle contains silicon besides aluminium. It indicates that some sites of aluminium and oxygen atoms are substituted by silicon and nitrogen atoms in the crystal structure of α-Al_2O_3. It can be said that the trapped particle is actually another oxynitride phase which possesses the same hexagonal crystal structure as α-Al_2O_3. Based on ionic valency balance, the following substitution is suggested to

TABLE III Spacings d between lattice planes determined from the electron diffraction pattern of the trapped particle and the corresponding standard values.

	Lattice plane		
	1	2	3
Determined d (nm)	0.4320	0.2352	0.2090
Standard d (nm)	0.433	0.2379	0.2085
Crystal planes	(0 0 0 3)	(1 $\bar{2}$ 1 0)	(1 $\bar{2}$ 1 3)

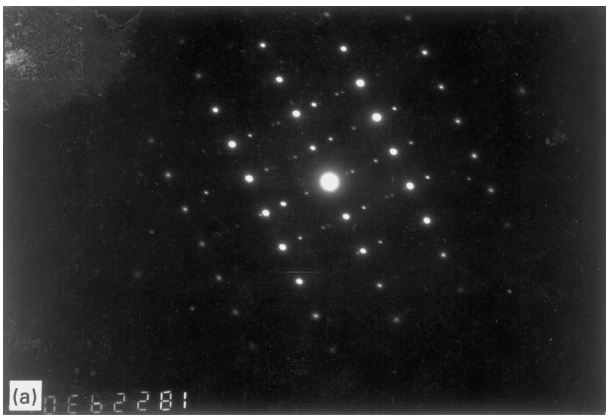

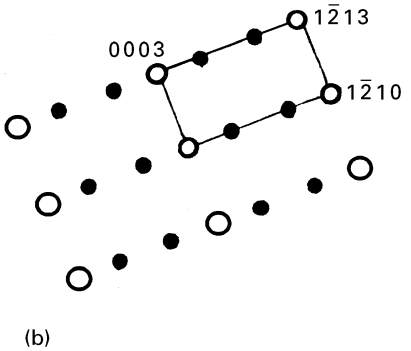

Figure 6 (a) The electron diffraction of the trapped particle in the [2 1 3 0] direction. (b) Corresponding index.

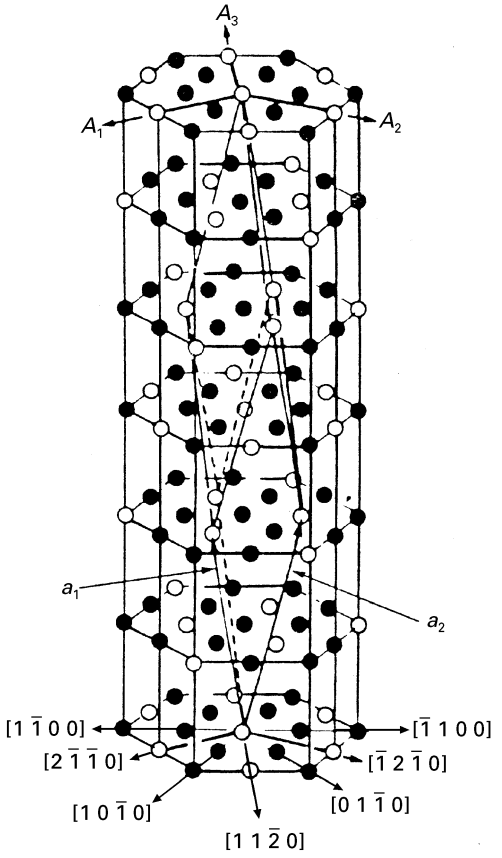

Figure 7 Arrangement of aluminum ions in a unit cell of α-Al_2O_3.

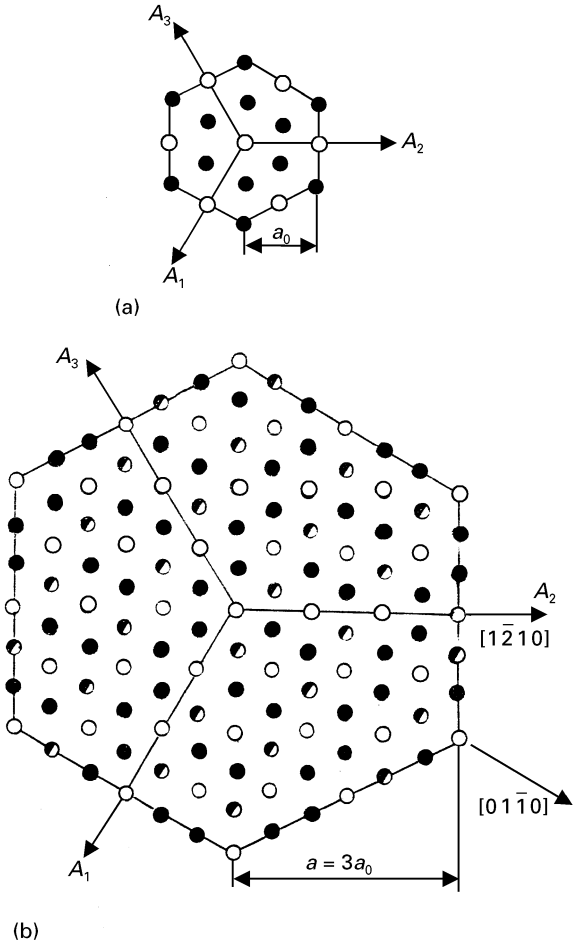

Figure 8 Relationship between the α-Al_2O_3 lattice and the superlattice of the trapped particle. (○) Silicon atom, (●) aluminium atom, (○) unoccupied site.

form the ordered solid solution to keep electron neutrality

$$Si_3N_4 + SiO_2 \xrightarrow{Al_2O_3} 4Si_{Al}^{0} + 4N_0' + 2O_0^x \quad (1)$$

A certain amount of SiO_2, which presumably originates from the surface of Si_3N_4 nanoparticles severely contaminated with oxygen, is required to form the oxy- nitride phase.

In the electron diffraction pattern of the trapped particle shown in Fig. 6, a group of weaker spots is observed, which corresponds to an additional period of three times the original period along the [1 2 1 0] direction (A_1, A_2 or A_3 axis direction). But no additional period exists in the Z-axis direction due to the absence of additional diffraction spots in the [0 0 0 3] direction. Therefore, the parameters of the superlattice may be written as follows in terms of the parameters of $\alpha - Al_2O_3$

$$a = 3a_0 = 1.43\ \text{nm} \quad (2)$$

$$Z = Z_0 = 1.30\ \text{nm} \quad (3)$$

The arrangement of aluminium atoms within a unit cell of α-Al_2O_3 is shown in Fig. 7 and a schematic presentation of the crystal structure of the ordered solid solution is shown in Fig. 8 in which partial sites of aluminium atoms are occupied by silicon atoms. It is evident that one-third of aluminium atoms and one-third of oxygen atoms are substituted by silicon and nitrogen atoms and the nominal chemical formula of this ordered solid solution phase can be written as $Al_4Si_2O_7N_2$. Further study needs to be undergone to confirm this new phenomenon.

4. Conclusions

1. A 15 vol% Si_3N_4/Al_2O_3 nanocomposite has been fabricated with the matrix grains in the shape of elongated columns, the aspect ratio of which was found to be in the range 2.5–4. The presence of liquid phase during sintering leads to the formation of column-shaped grains.

2. Two kinds of nanometre-sized particles are dispersed in the Al_2O_3 matrix. Comparatively larger particles in a small quantity are distributed at grain boundaries, and are identified to be β'-Sialon. An overwhelming quantity of smaller particles are trapped within the matrix, and are proved to be an ordered solid solution of Si_3N_4 in Al_2O_3. The trapped particles show an oxynitride phase which has a structure of α-Al_2O_3 with partial sites of aluminium and oxygen atoms occupied by silicon and nitrogen atoms.

3. The mechanical properties of the nanocomposite are markedly improved by the addition of nanoparticles, which can be attributed to the change of fracture mode from intergranular fracture to transgranular fracture, the "self-reinforcement effect" of the

elongated matrix grains, as well as a possible "pinning effect" of the intergranular particles.

References

1. I. LEVIN, W. D. KAPLAN, D. G. BRANDON and A. A. LAYYOUS, *J. Am. Ceram. Soc.* **8** (1995) 254.
2. G. PEZZOTTI and M. SAKAI, *ibid.* **77** (1994) 3039.
3. Y. SAKKA, D. D. BIDINGER and H. A. AKSAY, *ibid.* **78** (1995) 479.
4. L. C. STEARNS, J. H. ZHAO and M. P. HARMER, *J. Eur. Ceram. Soc.* **10** (1992) 473.
5. K. NIIHARA, K. SUGANUMA, A. NAKAHIRA and K. IZAKI, *J. Mater. Sci. Lett.* **9** (1990) 589.
6. K. NIIHARA, *J. Ceram. Soc. Jpn* **99** (1991) 974.
7. H. SONG and R. L. COBLE, *J. Am. Ceram. Soc.* **73** (1990) 2047.
8. L. A. XUE and I. W. CHEN, *ibid.* **74** (91) 2011.
9. J. H. GAO, Z. J. SHEN and Z. S. DING, *Chin. J. Mater. Res, Suppl. Issue* **8** (1994) 171.
10. K. NIIHARA and A. NAKAHIRA, *Mater. Sci. Monogr.* **68** (1991) 637.
11. J. H. GAO, Z. J. SHEN and Z. S. DING, in "Proceedings of the 1992' C-MRS Meeting" Guangzhou, China (1992) p. 448.

Received 12 January
and accepted 15 December 1995